
ACOUSTIC SIGNALS PROCESSING.
COMPUTER SIMULATION

Estimation of the Thickness Profile of a Human Skull Phantom by Ultrasound Methods Using a Two-Dimensional Array

S. A. Asfandiyarov^{a, *}, P. B. Rosnitskiy^a, S. A. Tsysar^a, P. V. Yuldashev^a, V. A. Khokhlova^a,
V. E. Sinitsyn^b, E. A. Merzhina^b, and O. A. Sapozhnikov^a

^a Physics Faculty, Moscow State University, Moscow, 119991 Russia

^b Medical Research and Education Center, Moscow State University, Moscow, 119991 Russia

*e-mail: asfandiyarov.sa14@physics.msu.ru

Received May 7, 2022; revised August 3, 2022; accepted September 22, 2022

Abstract—The paper presents the results of evaluating the thickness profile of a skull phantom using a two-dimensional ultrasound array consisting of piezoelectric elements with a center frequency of 2.1 MHz. Two pulse-echo ultrasound methods were used in the experiment: the A-mode elementwise measurements and scanning with a focused probing beam created by the entire array using delay-and-sum (DAS) beamforming. The obtained thickness profiles are compared with the reference thickness profile obtained using X-ray computed tomography. It was shown that ultrasound DAS beamforming with a focused probing beam makes it technically possible to estimate the thickness profile of the skull phantom.

Keywords: ultrasound imaging, inhomogeneous media, two-dimensional array, skull, brain, delay-and-sum beamforming

DOI: 10.1134/S106377102270004X

INTRODUCTION

Ultrasound (US) pulse-echo imaging methods are actively used for imaging human soft tissue. US imaging of brain structures through an intact skull is of particular interest [1, 2]. Currently, transcranial US imaging is feasible only through a limited number of acoustic windows. The inhomogeneity of the skull thickness, in which the speed of sound differs significantly from the speed of sound in soft tissues, in combination with strong acoustic attenuation in bones, lead to ultrasound wave weakening and strong refraction limiting the capabilities of transcranial imaging of the brain [3, 4]. The effect of refraction can be compensated using a two-dimensional antenna array by applying signals to its radiating elements with certain time delays [5, 6] or by introducing appropriate delays when processing the received echo signals. The acoustic delays introduced by the skull can be calculated from skull thickness profile data, obtained using computed tomography (CT). However, the most promising for the development of transcranial US imaging are methods that use only US techniques to develop a model of the skull and subsequent images of structures beyond it [7]. Therefore, the problem of developing a US pulse-echo methods for measuring the skull thickness profile is very important. The paper considers two pulse-echo approaches to solving this problem: the A-mode elementwise measurements and scanning the phantom

with a focused probing beam created by the entire array using delay-and-sum (DAS) beamforming [8].

MATERIALS AND METHODS

Skull Phantom

Experiments were performed using a skull phantom (Fig. 1a) made from a compound of epoxy resin and 30 wt % Al_2O_3 powder. Phantoms of such materials are often used in studying US propagation through skull bones [9]. The phantom was a 110×110 mm square plate, one side of which was smooth and flat; the other side was embossed so that the plate thickness varied in the range from 2 to 9 mm, which is typical for human skulls.

The thickness profile of the skull phantom was reconstructed from the CT datasets, obtained with a SOMATOM Drive Scanner (Siemens Healthineers, Germany) of the Medical Research and Education Center of Moscow State University. As a result of the CT scanning, a 3D model of the plate under study was built with a spatial resolution (voxel size) of $0.33 \times 0.33 \times 0.5$ mm.

To measure the speed of sound and attenuation coefficient in the epoxy resin– Al_2O_3 powder compound, in addition to the plate with varying thickness, a plane-parallel plate was made from the same material. The sample was a parallelepiped with sides of

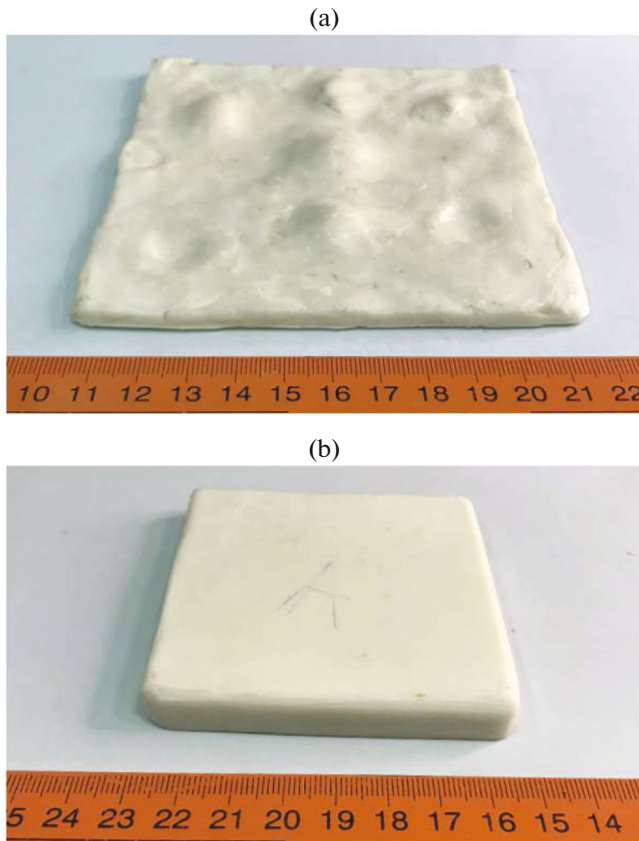


Fig. 1. Photographs (a) of the skull phantom and (b) reference sample used for measuring sound speed. These samples were made of an epoxy resin– Al_2O_3 powder compound.

$80 \times 80 \times 10$ mm (Fig. 1b). The speed of sound in the plate was determined using the substitution method [10], which measures the delay time of short US pulses passing from an emitter to a receiver in a reference medium (water) with and without the presence of such plane-parallel sample. Figure 2 shows a photograph of the experimental setup. Receiver 1 and emitter 2 are two identical Panametrics A392S-SU broadband piezoelectric transducers (Olympus NDT Inc., USA) with a diameter of $d = 38$ mm and center frequency of $f_c = 1$ MHz. The piezoelectric transducers were mounted on two metal frames on a rail base 3. The inclination of the frames was controlled with a screw, which made it possible to ensure plane-parallelism of the piezoelectric transducers. Sample 4 was placed between the emitter and receiver parallel to their surfaces using a special clamp. A JSR Ultrasonics DPR300 high-voltage pulser/receiver (Imaginant Inc., USA) was used to excite and receive short US pulses. The signals from the pulser/receiver were digitized with a TDS5054B oscilloscope (Tektronix Inc., USA). The measured speed of sound in the sample was 2620 ± 30 m/s; the attenuation coefficient was $\alpha = 220 \pm 20$ m^{-1} at the frequency of 2 MHz, corre-

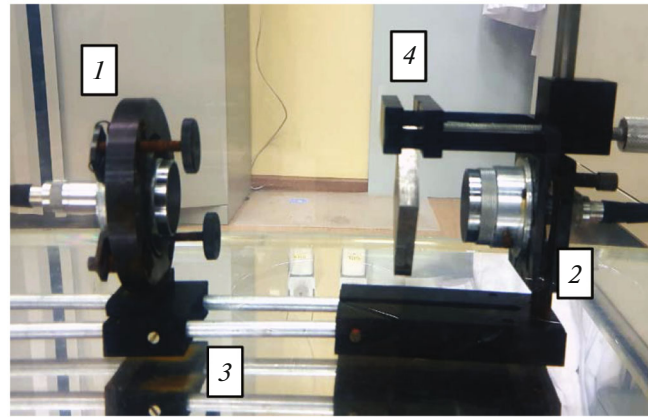


Fig. 2. Photograph of the experimental setup for measuring sound speed by displacement method: (1) emitter; (2) receiver; (3) rail base; (4) studied sample.

sponding to the results obtained earlier for this material [11].

Ultrasound System

For ultrasound-based measurement of the thickness profile of the skull phantom, a two-dimensional US array in the form of a plane square matrix with 20×20 cells containing piezoelectric elements (Medelkom, Lithuania) was used (Fig. 3). Each cell of the matrix was a square-shaped piezoelectric element with sides of $a_0 = 1.45$ mm. The element spacing (kerf) was 0.05 mm. In the array, 384 of the 400 elements were active. These active elements were divided into three groups of 128 elements. Each of these groups was controlled by a separate cable connected to a V-1 multichannel programmable electrical signal control system (Verasonics Inc., USA). The arrangement of the array elements on the surface is shown in Fig. 3b; the three groups of elements are marked A, B, and C. The center frequency of the piezoelectric elements in the transceiver mode at the minimum value of the reactive component of the impedance ranged from 1.9 to 2.3 MHz. To study the structure of vibrations of the array surface, broadband vibrometry was conducted beforehand using the acoustic holography method, the results of which are described in detail in [12].

Figure 4 shows a photograph of the experimental setup. The measurements were carried out in a tank of degassed water. The array 1 and the skull phantom 2 were fixed plane-parallel using the special clamps about 20 mm from each other for A-mode scanning and 80 mm for US imaging by delay-and-sum beamforming with a focused probing beam. In both cases, the smooth side of the phantom was facing the array. The phantom clamp was mounted on a UMS-3 positioner (Precision Acoustics, UK), which made it possible to move the phantom with respect to the array. This feature was used to match the thickness profile of

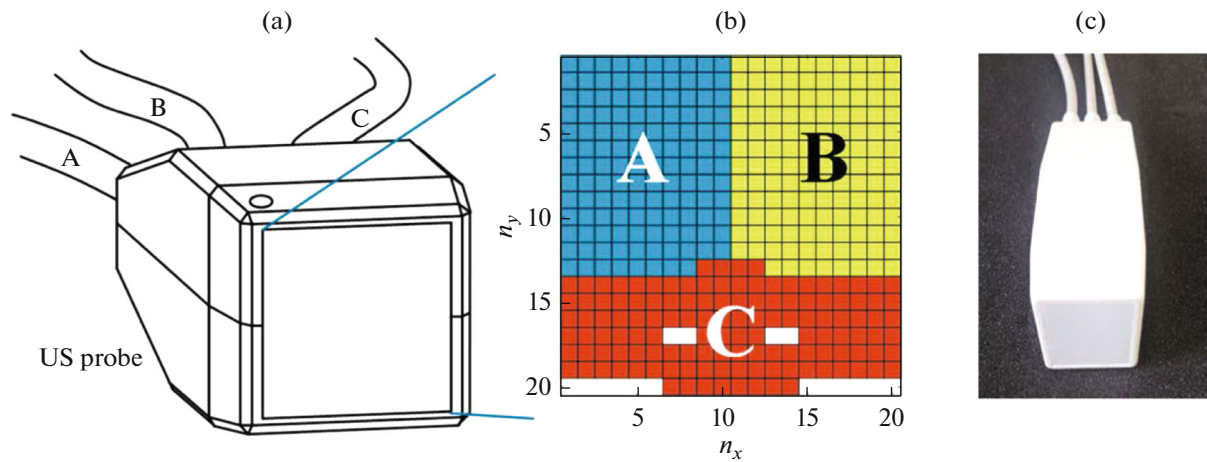


Fig. 3. (a, c) Two-dimensional US probe. Working area, 30×30 mm. (b) Arrangement of 384 piezoelectric elements on the front surface of the probe, divided into three sectors A, B, and C with 128 channels each.

the phantom obtained from US measurements with the 3D model obtained from the CT results: the sample was placed opposite the array using plane-parallel transfer such that one of the plate corners was opposite the array. Then, by constructing a C-mode US image in the plane of the smooth face of the sample, an image of the corner of the phantom was obtained; its coordinates with respect to the two-dimensional array and angle of rotation in the array plane were also determined. Further movements of the skull phantom with the positioning system were referenced to this position of its corner.

Ultrasound Methods for Estimating of the Thickness Profile of the Skull Phantom

One US method for estimating the thickness profile of the skull phantom was element-by-element scanning in the A-mode [13]. In such an assessment, each array element alternately emitted a US pulse of 4 cycles at a frequency of 2.1 MHz, then received the reflected signal. Figure 5 shows examples of the temporal profiles of the received signals for two different array elements. The black dotted line shows the received signals sampled at 8.4 MHz, and the black solid line shows their envelopes. The signal envelope was calculated as the absolute value of the analytical signal obtained from the received raw signals using the Hilbert transform. Figure 5a shows two local maxima of the envelope at 27 and 30 μ s, which correspond to the reflection of US pulses from the water–phantom (closest to the array) and phantom–water interfaces.

The measurements showed that the two local maxima of the envelope were not distinctly offset in all received signals (Fig. 5b). One of the reasons the maxima of the envelopes could not be separated was the low longitudinal image resolution, which is determined by the duration of the probing pulse. This reso-

lution was about 1.5 mm and therefore was comparable to the thickness of the thinnest parts of the skull phantom (~ 2 mm). In these areas, the echo pulse reflected from the far side of the phantom was superimposed on the tail of the pulse reflected from the near side, and therefore could not always be isolated (i.e. it was masked). Such masking could be further amplified by suppression of the amplitude of the second pulse due to irregularities on the far side of the phantom, which in some cases reflected the pulse to the side rather than strictly backwards. In addition, when the US pulse passes through an 8-mm-thick section of a skull phantom, its amplitude decreases by a factor of 6 (attenuation coefficient $\alpha = 220 \pm 20$ m $^{-1}$ at a frequency of 2 MHz). This signal level is still higher than the noise level by two orders of magnitude, but it is comparable with the level of the tail of the pulse (Fig. 5). To solve the masking problem, the fact that the reflective surface closest to the array was smooth and flat was

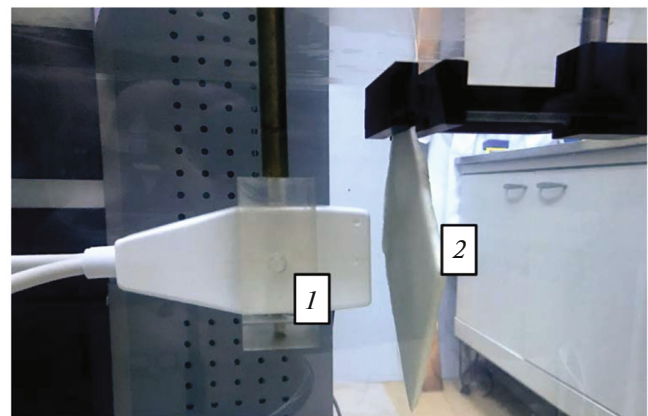


Fig. 4. Photograph of the experimental setup for US measurement of thickness profile of the skull phantom: (1) two-dimensional array; (2) skull phantom.

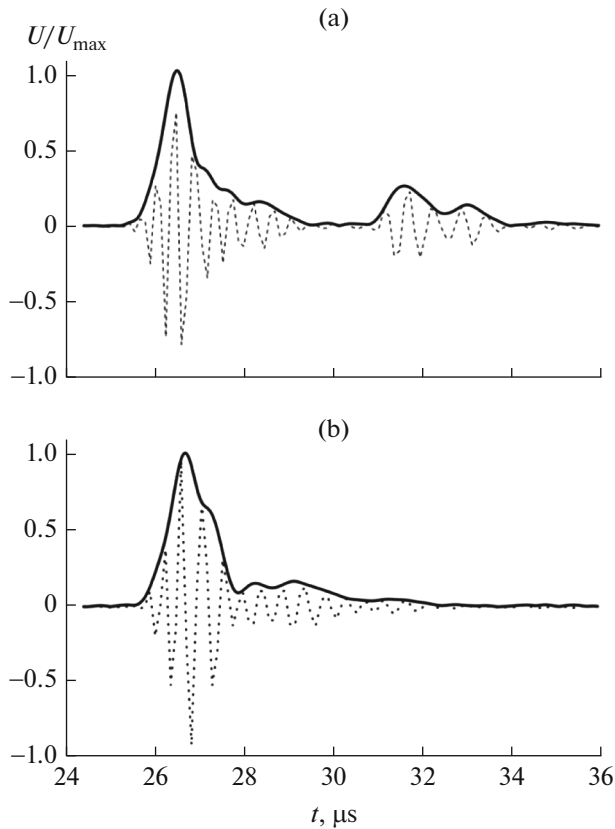


Fig. 5. Signal profiles U taken on different array elements (black dotted line), normalized to the maximum value U_{\max} . (a) Signal with well-distinguishable pulses, (b) signal with poorly distinguishable pulses. Black line shows signal envelopes.

used. This made it possible to assume that the shape of the first echo pulse was the same as in the case of reflection from a half-space flat boundary; therefore, to isolate the second echo, we were able to subtract the first echo from the received signal. The shape of the first reflected pulse for each array element was obtained experimentally by sequentially emitting a US pulse from each element and receiving the reflected pulses from the boundary of the thick plane-parallel sample of the same material made to measure the sound speed (see above). After subtraction, one local maximum was indeed distinguished, which presumably corresponded to reflection of the probing pulse from the phantom–water interface. As a result of processing this echo signal, the times corresponding to reflections of the US pulse from the water–phantom (t_1) and phantom–water (t_2) interfaces were determined. The thickness h of the phantom along the selected imaging axis was found as

$$h = \frac{c_s(t_2 - t_1)}{2}, \quad (1)$$

where $c_s = 2620 \pm 30$ m/s is the speed of sound in the skull phantom material.

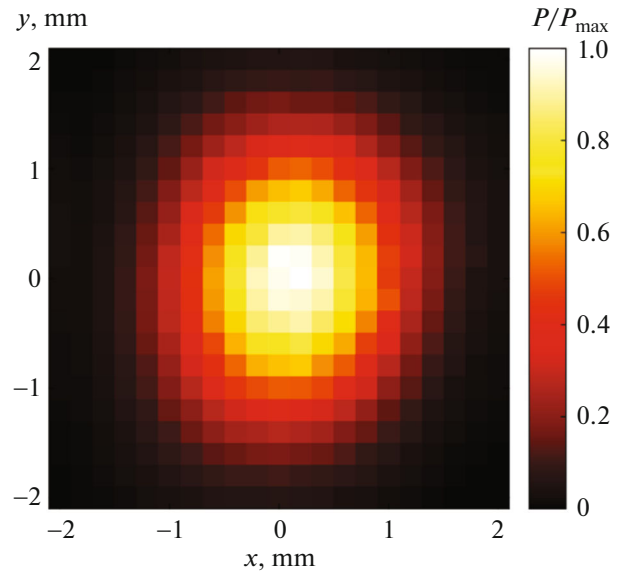


Fig. 6. Distribution of acoustic pressure amplitude $P(x, y)$ in the focal plane created by two-dimensional array at the distance of 80 mm from array surface using electronic focusing.

The second US method for estimating the thickness profile of the skull phantom was a pulse-echo scanning with a focused probing beam created by the entire array using DAS beamforming. In such assessment, electrical pulses were applied to the array elements with certain time delays, which made it possible to electronically focus the emitted US beam to a given point in space. The beam was focused sequentially at the points on the surface of the skull phantom, which were located at the nodes of a square grid of 10×10 points with resolution of 3 mm, i.e., at 100 points in a 30×30 mm square area. This choice of grid spacing was due to the transverse dimensions of the focal spot, $d \approx 3$ mm at the level of 0.15 of the maximum created by the two-dimensional array with electronic focusing at a distance of 80 mm (Fig. 6). The acoustic field was scanned in the focal plane using HNA-0400 needle hydrophone (Onda Corp., USA) with a sensor area of 0.4 mm in diameter. A micropositioning system allowed the hydrophone to be moved in the focal plane with a step of 0.2 mm along the x and y axes.

Raw US signals reflected from the phantom were received by all array elements and were subjected to quadrature processing [13] using a fifth-order Butterworth filter. The obtained quadrature components of the signal were used to construct the brightness distribution of the US image along the beam using DAS beamforming method. When summing the signals, the directivity pattern of the array elements was taken into account in the approximation of a piston radiator in a screen with soft walls [8]. The summation included signals coming from scatterers located in the directiv-

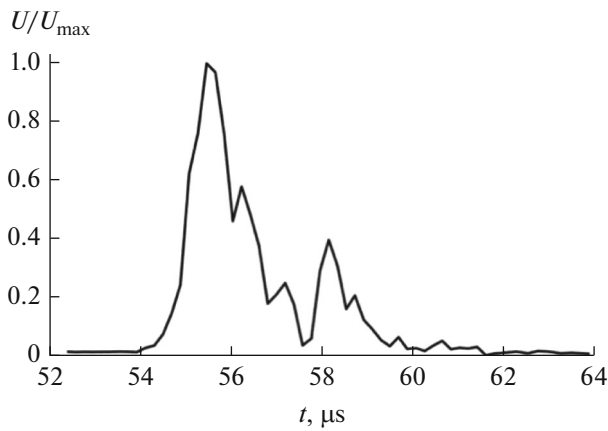


Fig. 7. Brightness distribution U of US image obtained by DAS beamforming method along one scan line perpendicular to the surface of two-dimensional array, normalized to the maximum value U_{\max} .

ity distribution within the level higher than 0.71 from the maximum level of the directivity diagram.

Since we were only interested in measurements close to the skull phantom, the amplitude of the echo signals was calculated only within a 20-mm-long segment of the image line, which included points, which corresponded to the position of the phantom. For each of the mentioned 100 probing points, the distribution of the echo signal amplitude was constructed, i.e., the brightness distribution of the US image was obtained in a volume of $3 \times 3 \times 20$ mm. The imaging results were then combined into a single volume of $30 \times 30 \times 20$ mm; i.e., in fact, a three-dimensional US image of the zone of interest was compiled.

Figure 7 shows an example of the brightness distribution of the US image along one of the scanning lines perpendicular to the flat side of the phantom. The distribution has two distinct local maxima at times $t_1 = 55.5 \mu\text{s}$ and $t_2 = 58 \mu\text{s}$, which presumably correspond to the reflection of US pulses from the water–phantom (closest to the array) and phantom–water interfaces. In contrast to the first US profiling method, pairs of such distinct local maxima were observed at the vast majority of points in the scanning area. Application of the equation (1) to times t_1 and t_2 obtained from the brightness distributions on the scanning line for different transverse coordinates made it possible to obtain the thickness profile: $h = h(x, y)$.

RESULTS AND DISCUSSION

In Fig. 8, colors represent thickness profiles $h(x, y)$ of the examined part of the skull phantom obtained by (a) CT and (b) the US elementwise scanning method. Each pixel of the distribution obtained with the US method corresponds to the thickness value $h(x, y)$ of the phantom opposite a specific array element. The pixel size of 1.45×1.45 mm is determined by the size of the array elements; their location corresponds to the arrangement of the array matrix (Fig. 3b), so there are voids in the image opposite the four inactive areas of the array surface.

Both thickness profiles (Figs. 8a, 8b) have a distinct thickness maximum of about 8 mm in the upper right corner, but the positions of this maximum differ by about 5 mm. The size of the area with a large h value surrounding the local maximum in the case of the US method is smaller than that of the maximum on the

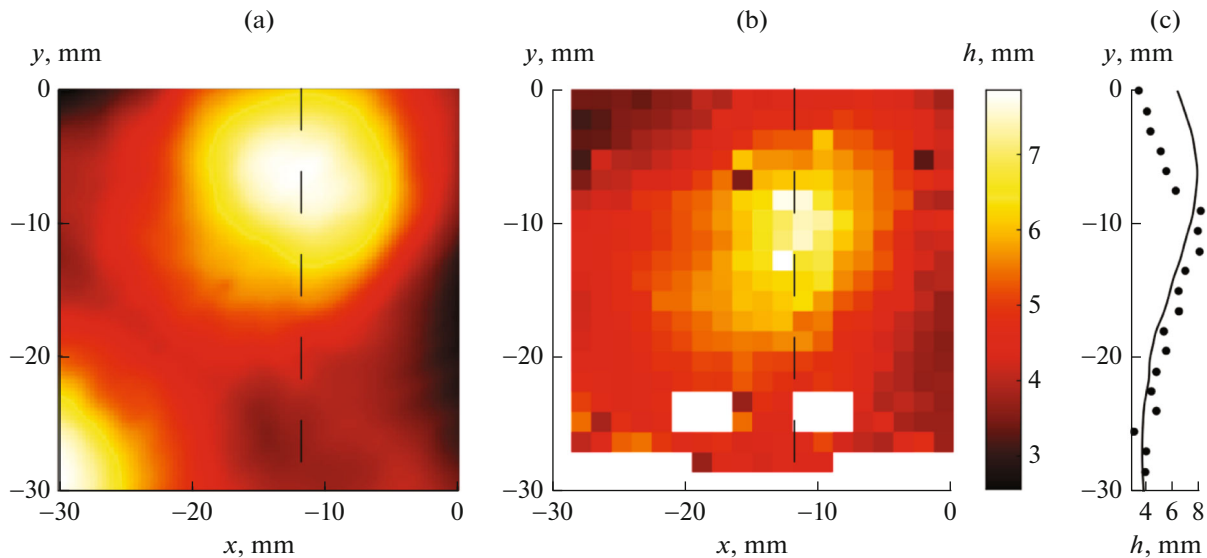


Fig. 8. Measured thickness profiles $h(x, y)$ of the skull phantom obtained using (a) CT and (b) US elementwise scanning method. (a, b) Dashed line shows straight line $x = -12$ mm, along which (c) one-dimensional thickness profile is constructed $h(x = -12 \text{ mm}, y)$; dots show profile measured by US method; solid line shows the profile measured by CT method.

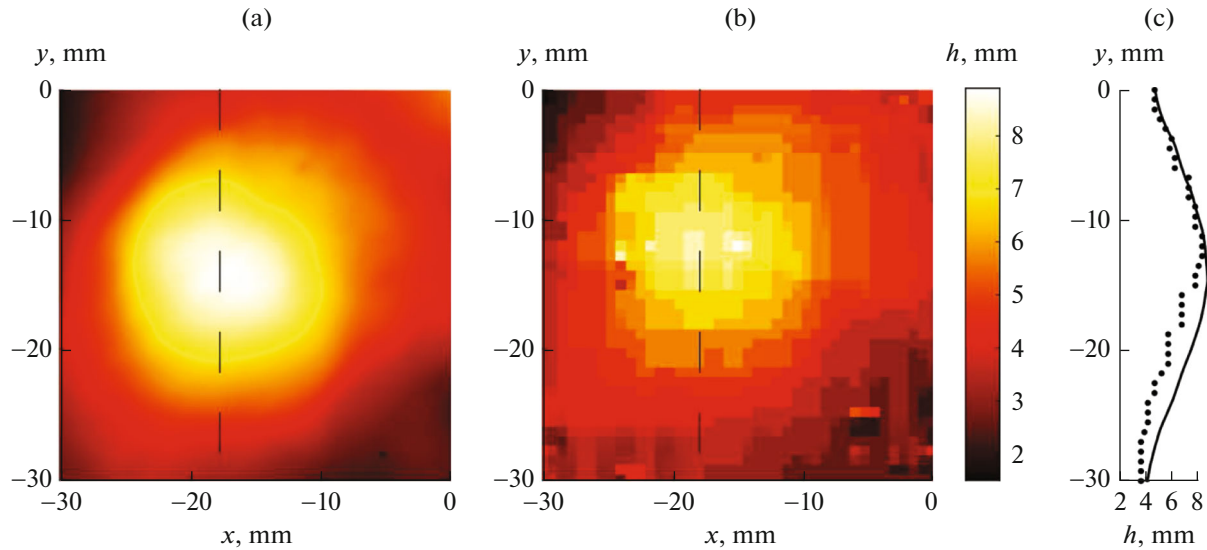


Fig. 9. Measured thickness profiles $h(x, y)$ of the skull phantom obtained using (a) CT and (b) US DAS beamforming with focused probing beam. (a) and (b) Dashed line shows straight line $x = -18$ mm, along which (c) one-dimensional thickness profile is constructed $h(x = -18$ mm, $y)$; dots show profile measured by US method; solid line shows the profile measured by CT method.

distribution obtained using CT. This may be due to the strong diffraction divergence of the beam emitted by the array elements. The half-angle of beam divergence from each element ($2\lambda/\pi a_0$, $\lambda = 0.75$ mm for a frequency of 2 MHz) is about 20° ; therefore, reflection from the phantom–water interface occurs not only from the point of the phantom located on the scanning line of the array element, but also from points shifted some distance transverse to the scanning line, where the sample thickness is already smaller. In this case, the reflected pulse will return to the array element earlier than for the reflection from a point located on the scanning line of the element. On the distribution obtained using CT, another local maximum in the lower left corner absent on the US distribution can be seen, which may also be associated with the diffraction divergence of the ultrasound beam. On the thickness profiles (Figs. 8a, 8b), the dashed line shows the straight line $x = -12$ mm, along which a one-dimensional thickness profile is constructed $h(x = -12$ mm, $y)$ (Fig. 8c); dots show the profile measured by the US method, and the solid line corresponds to the profile measured by the CT method.

In Fig. 9, colors represent thickness profiles $h(x, y)$ of the examined part of the skull phantom obtained by (a) CT and (b) pulse-echo measurements using a focused US beam created by DAS beamforming. In contrast to the first US profiling method, the second US method constructs a 3D image using DAS beamforming; therefore, it is possible to estimate the profile of the skull phantom in the entire studied area of 30×30 mm with a smaller pixel size of 0.75×0.75 mm, the distance between which is determined by the beam scanning step. The thickness profiles (Figs. 9a, 9b) are close to each other both in structure and plate thick-

ness. Both have a distinct maximum thickness of ~ 8 mm. The positions of this maximum agree well with each other, differing only by ~ 2 mm along the y axis. This slight shift in the distributions can be explained by the inaccurate placement of the 3D model obtained by the CT method in the coordinate system in which the US image was compiled. On the thickness profiles (Figs. 9a, 9b), the dashed line shows the straight line $x = -18$ mm, along which a one-dimensional thickness profile is constructed $h(x = -18$ mm, $y)$ (Fig. 9c); dots show the profile measured by the US method, and the solid line, the profile measured by the CT method.

CONCLUSIONS

In this study, two US methods were proposed and used to estimate the thickness profile of a skull phantom. The results were compared with a 3D model of the phantom obtained from CT datasets. The difference in the results when using A-mode elementwise scanning may be due to the diffraction divergence of the beam emitted by the array elements, as well as to large attenuation in the phantom material. In addition, the A-mode element-by-element scanning has a limited longitudinal resolution. Focusing of ultrasound probe signals using an entire two-dimensional array by introducing phase delays on its elements made it possible to increase the resolution and diminish the problem of diffraction divergence. The US method for estimating the thickness profile using DAS beamforming to create a focused probing beam made it possible to obtain more accurate results *versus* the elementwise scanning method. The sufficiency of the

obtained accuracy for calculating phase delays is a subject for further research.

FUNDING

The study was supported by the Russian Science Foundation (grant no. 19-12-00148) and by the Scientific and Educational School of Moscow State University “Photonic and Quantum Technologies: Digital Medicine.”

REFERENCES

1. S. Purkayastha and F. Sorond, *Semin. Neurol.* **32** (4), 411 (2012).
2. D. Antipova, L. Eadie, A. S. Macaden, and P. Wilson, *Ultrasound J.* **11** (29), 1 (2019).
3. S. V. Baikov, A. M. Molotilov, and V. D. Svet, *Acoust. Phys.* **49** (3), 276 (2003).
4. S. V. Baykov, L. V. Babin, A. M. Molotilov, S. I. Neiman, V. V. Riman, V. D. Svet, and A. I. Selyanin, *Acoust. Phys.* **49** (4), 389 (2003).
5. G. T. Clement, J. Sun, T. Giesecke, and K. Hynynen, *Phys. Med. Biol.* **45** (12), 3707 (2000).
6. M. Pernot, J.-F. Aubry, M. Tanter, J.-L. Thomas, and M. Fink, *Phys. Med. Biol.* **48** (16), 2577 (2003).
7. A. Wydra, E. Malyarenko, K. Shapoori, and R. Gr. Maev, *Phys. Med. Biol.* **58** (4), 1083 (2013).
8. V. Perrot, M. Polichetti, F. Varray, and D. Garcia, *Ultrasonics* **111**, 106309 (2021).
9. A. Wydra and R. Gr. Maev, *Phys. Med. Biol.* **58** (22), N303 (2013).
10. M. Bakaric, P. Miloro, A. Javaherian, B. T. Cox, B. E. Treeby, and M. D. Brown, *J. Acoust. Soc. Am.* **150** (4), 2798 (2021).
11. L. I. Gil'fanova, S. A. Tsysar', P. V. Yuldashev, and V. D. Svet, *Uch. Zap. Fiz. Fak. Mosk. Univ.*, No. 4, 154322 (2015).
12. S. A. Tsysar', D. A. Nikolaev, and O. A. Sapozhnikov, *Acoust. Phys.* **67** (3), 320 (2021).
13. C. R. Hill, J. C. Bamber, and G. R. ter Haar, *Physical Principles of Medical Ultrasonics* (John Wiley & Sons, 2004; Fizmatlit, Moscow, 2008).